ELSEVIER

Contents lists available at ScienceDirect

Earth and Planetary Science Letters

journal homepage: www.elsevier.com/locate/epsl





Global oceanic basalt sources and processes viewed through combined Fe and Mg stable isotopes

Caroline R. Soderman ^{a,*}, Simon Matthews ^b, Oliver Shorttle ^a, Matthew G. Jackson ^c, James M.D. Day ^d, Vadim Kamenetsky ^e, Helen M. Williams ^a

- ^a Department of Earth Sciences, University of Cambridge, Cambridge, CB2 3EQ, UK
- b Institute of Earth Sciences, University of Iceland, Reykjavik, Iceland
- ^c Department of Earth Sciences, University of California Santa Barbara, CA 93106, USA
- ^d Scripps Institution of Oceanography, University of California San Diego, CA 92093-0244, USA
- ^e Centre of Deep Sea Research, Institute of Oceanology, Chinese Academy of Sciences, 266071 Qingdao, China

ARTICLE INFO

Editor: R. Hickey-Vargas

Keywords: Fe stable isotopes Mg stable isotopes mantle heterogeneity volcanic hotspots OIB

ABSTRACT

Oceanic basalts show variation in their iron and magnesium isotope compositions. One hypothesis for the origin of this is source variation: radiogenic isotope and trace element abundance studies have long argued that the Earth's upper mantle is geochemically heterogeneous and that subducted crust is a major contributor to this diversity. In contrast, a recent hypothesis posits that stable isotopes record disequilibrium during melt transport and so provide novel insight into the melting process. In this study we investigate the first of these hypotheses, that source heterogeneity explains global Fe-Mg isotope systematics. We compile a global dataset of oceanic basalt Fe and Mg isotopes and complement this with new Fe-Mg isotope data from locations possessing some of the most extreme radiogenic isotope ratios for their setting: ocean island basalts from the Cook-Austral and Society islands and a Mid-Atlantic Ridge basalt. Despite both Fe and Mg isotope systems having the ability to trace recycled crustal material in the mantle, their global systematics are very different in this dataset. The global compilation of primitive oceanic basalts records heavier Fe (higher δ^{57} Fe) isotope compositions than bulk silicate earth (BSE), but a mixture of heavier and lighter Mg isotope compositions than BSE. By employing a coupled Fe-Mg equilibrium isotope fractionation model during mantle melting we show that much of this isotopic variability can be generated by the mixed melts produced by melting of peridotite mantle containing moderate amounts of recycled crust as a discrete lithology. The Fe isotope composition of the melts is controlled by the bulk isotope composition of the recycled crust (expected to be considerably heavier than BSE, but variable). In contrast, the Mg isotope composition is controlled by source mineralogy. Olivine-poor lithologies such as recycled crust are able to generate large Mg isotope fractionations during melting, both positive and negative (± 0.1‰) relative to the mantle source, depending on the presence of spinel, clinopyroxene or garnet. These melt Mg isotope fractionations are consistent with the Mg isotope compositions of mid-ocean ridge basalts generated by variable depths of mantle melting. Our equilibrium model provides a baseline to test hypotheses of Fe-Mg isotope variability in basalts: our results show that contributions from recycled crust-derived melts, generated in spinel-, pyroxene-, and garnet-bearing mineral assemblages in the mantle, would be able to produce much of the Fe-Mg isotope variability seen in the global compilation of primitive oceanic basalts, without requiring isotopically extreme mantle components (e.g., carbonate with a light Mg isotope signature) or disequilibrium fractionation. However some basalt variability in ocean island settings may indeed fall outside the paradigm of pyroxenite heterogeneity - whilst we consider carbonates unlikely to be important, disequilibrium processes may in these cases play a role.

1. Introduction

Over the past decade, measurements of Fe and Mg stable isotopes have been evaluated as tracers of recycled crust in the mantle sources

https://doi.org/10.1016/j.epsl.2024.118749

^{*} Corresponding author.

E-mail address: cs801@cam.ac.uk (C.R. Soderman).

of oceanic basalts (e.g., Williams and Bizimis, 2014; Konter et al., 2016; Zhong et al., 2017; Nebel et al., 2019; Gleeson et al., 2020; Soderman et al., 2021, 2023), in complement to other observations such as major and trace elements in basalts and their olivine crystals, and radiogenic isotope ratios. These stable isotope systems, alongside others such as calcium and zinc, are also potential tracers of lithological heterogeneity through equilibrium inter-mineral isotope fractionation, which causes isotope fractionation during mantle melting and crystallisation (e.g., Williams and Bizimis, 2014; Macris et al., 2015). However, the global dataset of Fe and Mg isotope compositions of oceanic basalts show characteristic differences relative to bulk silicate earth, BSE (Fig. 1). Notably, nearly all primitive oceanic basalts have heavier Fe isotope ratios (i.e., higher δ^{57} Fe) than the estimated composition of BSE, whereas the Mg isotope ratios of oceanic basalts scatter to either side of the BSE value (Fig. 1). Within this global dataset of mid-ocean ridge basalts (MORB) and ocean island basalts (OIB) are localities with radiogenic isotope ratios at the end of the observed spectrum (e.g., Pitcairn, Samoa, St. Helena). The isotopic, major and trace element geochemistry of the global basalt compilation underpins our understanding of the mantle as a geochemically heterogeneous reservoir, with most of the geochemical diversity thought to originate from recycled oceanic crust, along with contributions from sediments and continental crust (e.g., Zindler and Hart, 1986; White and Hofmann, 1982; Chauvel et al., 1992; Hofmann, 1997; Willbold and Stracke, 2006; Jackson and Dasgupta, 2008; Shorttle and Maclennan, 2011; Stracke, 2012). However, there is an open question over the link between the Fe-Mg isotope composition of primitive oceanic basalts and this crust-derived geochemical heterogeneity: whether contributions from melts of recycled oceanic crust (pyroxenite) in the mantle can generate the Fe-Mg isotope variability seen in basalts through equilibrium isotope fractionation, or if there is a need to invoke either more exotic mantle sources, such as low δ^{26} Mg carbonate components (e.g., Wang et al., 2018; Shi et al., 2022), or further processes, such as disequilibrium isotope fractionation (Liu et al., 2023).

The offset of Fe isotope compositions in primitive oceanic basalts relative to BSE has generally been ascribed to an isotopically heavy mantle source component (compared to peridotite) combined with a small partial melting effect (e.g., Williams and Bizimis, 2014; Konter et al., 2016; Sossi et al., 2016; Nebel et al., 2019; Gleeson et al., 2020; Wang et al., 2021a; Soderman et al., 2021, 2023; Guo et al., 2023) which dominantly arises from the relative incompatibility of isotopically heavy Fe³⁺ compared to Fe²⁺ (Dauphas et al., 2014). Modelling suggests that the isotopically heavy mantle source component is mostly explained by the expected bulk δ^{57} Fe offset of pyroxenite relative to peridotite (Sun et al., 2020; Wang et al., 2021a; Soderman et al., 2021), rather than an equilibrium mineralogy-specific effect. However, partial melting of garnet-bearing pyroxenite has also been proposed to contribute to high δ^{57} Fe in OIB (Nebel et al., 2019) directly due to mineral-specific fractionation. Isotopically heavy sub-oceanic lithospheric mantle may also be produced during metasomatism by high δ^{57} Fe low-degree melts, and equilibrium isotope fractionation during melting of these lithospheric mantle sources could generate high δ^{57} Fe in basalts (Konter et al., 2016; Sun et al., 2020; Guo et al., 2023). Other Fe isotope variability in oceanic basalts could be caused by kinetic diffusion-driven processes, either via Fe diffusion between co-existing crystals and melt (e.g., Dauphas et al., 2010; McCoy-West et al., 2018, although the impact on the whole-rock scale may be small) or via melt-rock reaction during melt transport (Liu et al., 2023).

The generation of Mg isotope variability of primitive oceanic basalts relative to BSE has previously been ascribed to variable partial melting degrees of garnet-bearing lithologies, which might generate low $\delta^{26} \rm Mg$ melts (Zhong et al., 2017) if garnet is contributing significantly to melting. This fractionation occurs because garnet has low $\delta^{26} \rm Mg$ relative to other mantle minerals, due to high Mg coordination and long (hence weak) Mg–O bonds. By contrast, phases such as spinel and diopside have low Mg coordination and stronger Mg–O bonds than olivine (Wang et al., 2023). Therefore, partial melting could generate

positive or negative $\Delta^{26} \text{Mg}_{\text{melt}-\text{source}}$ depending on the residual mineralogy (Zhong et al., 2017). The combined effect of melting degree and source mineralogy may dominate the isotope composition of recycled crustal melts over any effect from the bulk δ^{26} Mg of recycled crust, since average MORB and BSE have similar δ^{26} Mg (Teng et al., 2010; Huang et al., 2011a; Stracke et al., 2018; Liu et al., 2023). Alternatively, the mantle source regions of oceanic basalts with higher $\delta^{26} \mathrm{Mg}$ than BSE, such as back-arc basalts from the South China Sea, may have been metasomatised by subduction-related fluids (e.g., Ding et al., 2022), and disequilibrium isotope fractionation during Mg diffusion associated with melt transport has been suggested to produce low $\delta^{26} \mathrm{Mg}$ melts (Liu et al., 2023). The $\delta^{26} \mathrm{Mg}$ of oceanic basalts may also be affected by unusual mantle source components, such as recycled marine carbonates (with δ^{26} Mg as low as $-5\%_0$, see Wang et al., 2018 and references within): subducted carbonates (or at least their Mg isotopic fingerprint) have been invoked to explain low $\delta^{26}{\rm Mg}$ in Pitcairn basalts by Wang et al. (2018). However, even when filtering out basalts with evidence for a carbonate-bearing mantle source (by removing samples with ${}^{87}\mathrm{Sr}/{}^{86}\mathrm{Sr} > 0.7044$, the threshold suggested by Huang et al. (2011a) for basalts with > 5% recycled ancient carbonate component in their mantle source), the global oceanic basalt dataset still shows considerable scatter in δ^{26} Mg to either side of BSE (Fig. 1).

The contrasting variability of Fe and Mg stable isotopes relative to BSE in global oceanic basalts, where mantle sources are known to be lithologically diverse and include recycled crust, mean that the two systems may be tracing different aspects of the sources and processes contributing to melt production in oceanic settings. To investigate the origin of the contrasting Fe and Mg isotope behaviour in oceanic basalts, and particularly to assess whether contributions from pyroxenite-derived melts can generate this variability, we present a model of combined equilibrium Fe-Mg stable isotope behaviour during mantle melting of peridotite and pyroxenite lithologies. Our model follows the approach of the thermodynamically self-consistent melting and equilibrium isotope fractionation models presented previously (Soderman et al., 2021, 2022), updated for Mg following new intermineral fractionation constraints (Liu et al., 2022; Wang et al., 2023). We then compare the model results with the global dataset of basalts which have both Fe and Mg isotope measurements on the same sample, along with new stable Fe-Mg isotope data for a selection of basalts from Pacific intraplate volcanoes and a Mid-Atlantic Ridge basalt. We use our combined results to explore the constraints on mantle source and process (e.g., lithology/mineralogy, depth of melting) that a combined Fe-Mg isotope approach can give and, indirectly, whether a new process such as disequilibrium isotope fractionation is required. We show that the presence of small amounts of recycled oceanic crust as a discrete lithology in the mantle can, by itself, generate much of the range in Fe and Mg isotope ratios seen in Pacific OIB, without needing to invoke the widespread presence of unusual mantle components such as recycled carbonates. Iron and Mg isotopes are therefore consistent with the picture of ambient upper mantle lithological heterogeneity derived from conventional major, trace element and radiogenic isotope tracers (e.g., Allègre and Turcotte, 1986; Hirschmann and Stolper, 1996; Jackson and Dasgupta, 2008; Shorttle and Maclennan, 2011). However, in some ocean island settings it may be difficult to generate the more extreme observed high δ^{57} Fe and/or low δ^{26} Mg basalt compositions through equilibrium isotope fractionation by melting of pyroxenitebearing mantle. These cases may point to additional processes operating to fractionate these isotopes, such as disequilibrium effects during melt transport (e.g., Liu et al., 2023).

2. Methods

2.1. Modelling isotope fractionation during mantle melting

To understand the behaviour of Fe and Mg isotopes during melting of peridotite and pyroxenite we use phase equilibria results combined

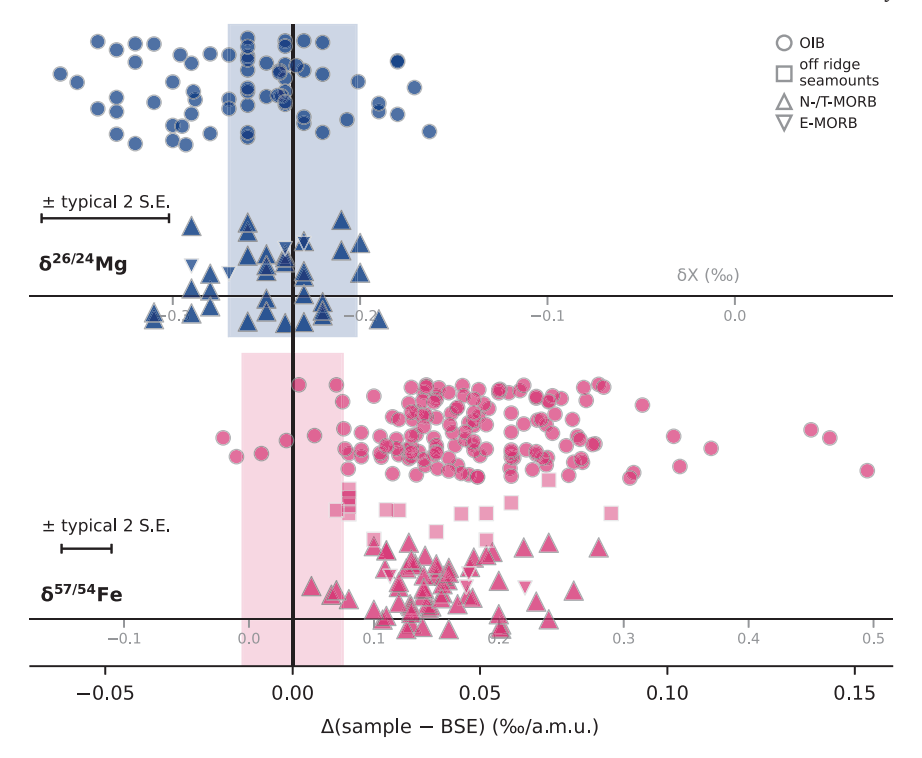


Fig. 1. Compilation of Fe and Mg isotope data in oceanic basalts (OIB, MORB). The data has been filtered to only include samples with MgO contents between 7 and 16 wt%, to limit the effects of fractional crystallisation or crystal accumulation on the isotope compositions recorded in the basalts. Where MORB type is known, samples are classified as N-/T- or E-type (as classified by Teng et al., 2013); if classification is not known, samples are plotted as N-/T-type. Where published data is available, Mg isotope data are filtered for basalts with 87 Sr/ 86 Sr < 0.7044; corresponding to < 5% carbonate in the mantle source, from Huang et al. (2011a). The main axis shows the variability in natural data from the BSE value for each isotope system, scaled by the difference in the atomic mass units (a.m.u.) of the isotopes being measured. The coloured bars show 2 S.D. on the BSE estimates. BSE values used are δ^{26} Mg = 0.24±0.03‰ (Liu et al., 2023), δ^{57} Fe = 0.035±0.04‰ (average of Sossi et al., 2016; Johnson et al., 2020). Data sources in the Supplementary Material.

with an equilibrium Fe-Mg isotope fractionation model which responds to changes in mantle mineralogy, temperature and pressure. The phase equilibria results and the Fe isotope fractionation model used are as presented in Soderman et al. (2021, 2022). The Mg isotope fractionation model is updated based on new *ab initio* estimates of equilibrium inter-mineral Mg isotope fractionation presented in Wang et al. (2023). The new fractionation factors are an improvement on those used in Soderman et al. (2022) as they represent a self-consistent set for all the minerals considered (i.e., all from one study) and include pressure as well as temperature dependence (see Supplementary Material).

For peridotite, we use the KLB1 composition (Davis et al., 2009). Natural mantle pyroxenites (olivine-poor, pyroxene-rich rocks) have a range of compositions from silica-excess to silica-deficient (Lambart et al., 2016), so following Soderman et al. (2022) we have chosen two pyroxenite compositions. One, silica-deficient MIX1G (Hirschmann et al., 2003), reflects the average of global pyroxenite lithologies observed from the mantle (Lambart et al., 2016), and which we subsequently use in Figs. 4, 5 & 7. The other, G2, is a silica-excess MORB-like pyroxenite composition (Pertermann and Hirschmann, 2003) and is shown in Fig. 3

We also discuss the effects of a potential non-zero $\Delta^{26} \mathrm{Mg}_{\mathrm{olivine-melt}}$. Some studies such as Stracke et al. (2018) are based on the assumption that there is no resolvable Mg isotope fractionation between olivine and silicate melt. However, Liu et al. (2022) have recently suggested that olivine is isotopically lighter than silicate melt, although their results obtained by modelling mantle melting using this fractionation factor produce high $\delta^{26} \mathrm{Mg}$ melts not generally observed in the natural dataset (Liu et al., 2023).

2.2. Samples

The existing dataset of oceanic basalts with both Fe and Mg isotope measurements on the same rock sample is relatively limited compared to the measurements of each separate isotope system. Therefore, we have selected eleven new oceanic basalt samples (ten OIB, one MORB) for Fe isotope analysis, and nine of these for Mg isotope analysis, that we can use to test of the results of our modelling. The samples were chosen based on having radiogenic isotope compositions consistent with the presence of recycled crust in their mantle source (Fig. 2). We focus mostly on Pacific OIB, to complement the existing (but limited) coupled Fe-Mg data on plume-related basalts from Hawai'i, Pitcairn, Louisville and the Society islands (Teng et al., 2008, 2010, 2013; Zhong et al., 2017; Wang et al., 2018; Shi et al., 2022).

We select samples from the Cook-Austral islands of Rarotonga and Aitutaki (focusing on late-stage lavas from Aitutaki), and the Society island of Tahaa. Rarotonga and late-stage Aitutaki lavas are thought to represent products of the putative Rarotonga hotspot (e.g., Chauvel et al., 1997; Jackson et al., 2020), with volcanism from < 2 Ma recorded in both islands. The samples used here are from this young volcanic activity; a distinct older stage of volcanism (9.5 Ma) has also been recorded in Aitutaki (Turner and Jarrard, 1982; Rose and Koppers, 2019). Instead of being the result of plume-fed hotspot volcanism, Rarotonga and the younger Aitutaki volcanism may also be a product of rejuvenated-style volcanism (Jackson et al., 2020), most resembling the enriched 'EM1' mantle endmember similar to that found in rejuvenated Samoan lavas (Workman et al., 2004; Jackson et al., 2014) in Sr-Nd-Pb isotope space.

Other Pacific plume tracks include Pitcairn, Samoa and the Society islands. The Society islands show an age progression from ~ 4 Ma to present day (White and Duncan, 1996). Some of the lavas erupted

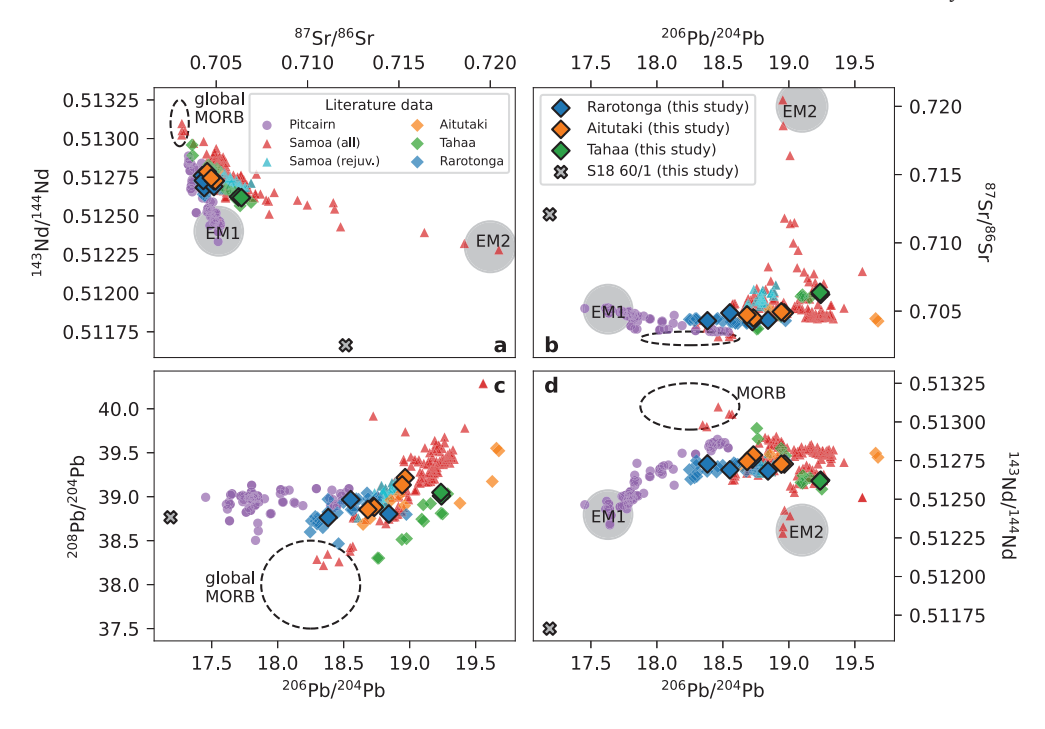


Fig. 2. Compilation of published radiogenic isotope data for some Pacific OIB and seamounts. Samples used in this study outlined in black; also shown (as grey cross) is an isotopically-extreme (extreme EM1-like) Atlantic MORB sample S18 60/1 (Kamenetsky et al., 2001) studied here. Data compiled from GEOROC https://georoc.eu/; detail in Supplementary Material. Also shown are the isotopic compositions of average global MORB (black dashed region; Stracke et al., 2005) and global mantle endmembers (grey ovals for EM endmembers: EM2 from Jackson et al. (2007), EM1 from Konter et al. (2008) and Stracke et al. (2005) for 208 Pb/204 Pb.

have radiogenic Sr and unradiogenic Nd isotope compositions, and intermediate Pb isotope compositions (White and Duncan, 1996), that are consistent with an enriched mantle source most closely resembling the 'EM2' endmember identified in Samoan shield lavas (Workman et al., 2004). Samples from the Society island of Tahaa have shield-stage lavas with the most extreme known EM2 isotopic compositions from the hotspot (White and Duncan, 1996). The Pitcairn plume occupies a distinct region of Sr-Nd-Pb isotope space away from the Society and Samoa shield lavas, instead defining the enriched mantle 'EM1' endmember with elevated ⁸⁷Sr/⁸⁶Sr and unradiogenic ²⁰⁶Pb/²⁰⁴Pb (e.g., Woodhead and Devey, 1993; Jackson and Dasgupta, 2008) (Fig. 2). Together, 'EM1' and 'EM2' are thought to be endmembers of a continuous mixing array of enriched mantle components reflecting inputs of recycled oceanic and continental crust and sediments to the mantle.

The selected samples from Rarotonga, Aitutaki and Tahaa form a spread in Sr-Nd-Pb isotope space (Fig. 2), and represent some of the most extreme EM1 and EM2 isotopic compositions amongst each island. Whole rock geochemistry for one Rarotonga basalt (RAR-B-9) and one Tahaa basalt (TAA-B-26) is published in Hauri and Hart (1993, 1997), and radiogenic isotope compositions for Rarotonga and Tahaa basalts are published in Hauri and Hart (1993). The whole rock geochemistry of the other Rarotonga and Tahaa samples, and radiogenic isotope composition of one Tahaa basalt, are presented here (Data S3). A petrographic summary of these samples can be found in the Supplementary Material. The full major and trace element concentrations, radiogenic isotope ratios, and petrographic descriptions of the Aitutaki basalts (which are nephelinites and a basanite block from a basaltic tuff breccia), are published in Jackson et al. (2020). All selected samples have 7 < MgO (wt%) < 17 to avoid those that have undergone extensive crystal accumulation or fractional crystallisation, particularly magnetite and Mg-bearing Fe-Ti oxide fractionation, which may affect both Fe and Mg isotope compositions of basalts (e.g., Williams et al., 2018; Su et al., 2019).

We also include a high MgO dredged glass sample (S18 60/1) from the southern Mid-Atlantic Ridge, whose unique geochemistry (HREE-

depletion, radiogenic Sr, unradiogenic Nd, Hf, low ²⁰⁶Pb/²⁰⁴Pb but relatively high ²⁰⁷Pb/²⁰⁴Pb) has been attributed to Precambrian garnet-bearing continental crustal material in its source region (Kamenetsky et al., 2001). Including this sample in the Fe-Mg isotope analysis allows us to further test the sensitivity of coupled Fe-Mg isotopes to mantle source lithology.

2.3. Analytical methods

All analyses were carried out following established methods (see Supplementary Materials). Bulk rock major-, minor- and trace-element abundance data were determined at the Scripps Isotope Geochemistry Laboratory, Scripps Institution of Oceanography. Strontium, Nd and Pb isotope measurements on basalt TAA-B-21 were determined at the University of South Carolina. Stable Fe and Mg isotope purification and analyses were carried out at the University of Cambridge. Iron isotope analyses were performed on a MC-ICP-MS NeptunePlus in wet plasma and medium resolution, with sample standard bracketing to the IRMM-014 standard. Iron isotope measurements are reported as

$$\delta^{57/54} \text{Fe} = \left(\frac{(^{57} \text{Fe}/^{54} \text{Fe})_{\text{sample}}}{(^{57} \text{Fe}/^{54} \text{Fe})_{\text{IRMM}-014}} - 1\right) \times 1000. \tag{1}$$

The international geological reference materials BHVO-2, BCR-2 and BIR-1 were used to evaluate column chemistry procedures, and the in-house FeCl₃ standard was used to assess mass dependence, reproducibility and accuracy. All give values in agreement with published values (Data S3).

Magnesium isotope analyses were performed on a MC-ICP-MS NeptunePlus in 'semi-dry' plasma (samples introduced via an Apex introduction system) and medium resolution, with sample standard bracketing to the DSM-3 standard. Isotope measurements are reported as

$$\delta^{26/24} Mg = \left(\frac{(^{26}Mg/^{24}Mg)_{sample}}{(^{26}Mg/^{24}Mg)_{DSM-3}} - 1 \right) \times 1000.$$
 (2)

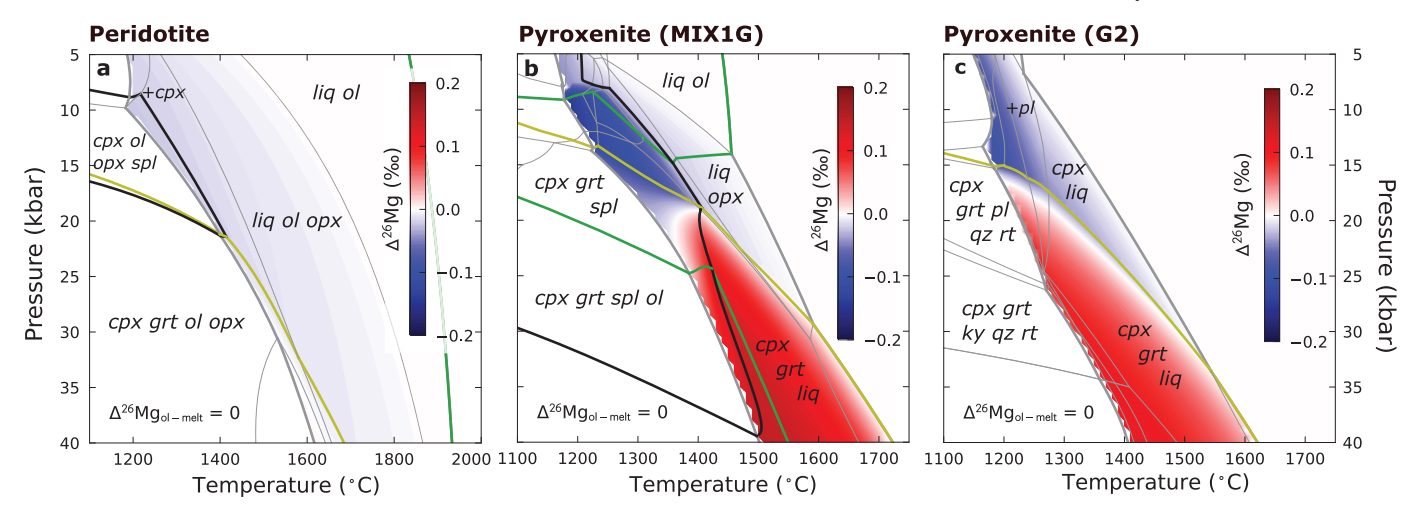


Fig. 3. Calculated magnesium isotope fractionation during partial melting of peridotite (KLB1) and pyroxenite (MIX1G & G2), following Soderman et al. (2021, 2022) with inter-mineral fractionation information updated from Wang et al. (2023). The appearance/disappearance of key mineral phases are marked: olivine (green), garnet (mustard), spinel (black). All melt isotopic fractionations are shown relative to a bulk source composition of 0 ‰. Mineral abbreviations: cpx = clinopyroxene, grt = garnet, ky = kyanite, ol = olivine, opx = orthopyroxene, rt = rutile, spl = spinel, qz = quartz.

The international geological reference material BHVO-2 and in-house synthetic standard CCSR3 were used to evaluate column chemistry procedures, and the in-house Cambridge-1 mono-elemental standard was used to assess mass dependence, reproducibility and accuracy. The results are in agreement with published values (Data S3).

3. Results

3.1. Modelling

The results of our updated mantle melting Mg isotope fractionation model, using the constraint as used in Soderman et al. (2022) of $\Delta^{26} \mathrm{Mg}_{\mathrm{olivine-melt}} = 0$, are shown in Fig. 3. We have calculated the isotope fractionation of the melt relative to the bulk source for peridotite and the two pyroxenites. The isotope composition of all phases is shown for reference in Figs. S3–S5. The main difference to the results from Soderman et al. (2022) is the increased magnitude of $\Delta^{26}\mathrm{Mg}_{\mathrm{mineral-source}}$ for the isotopically lightest and heaviest minerals, garnet and spinel respectively. The resulting melt compositions show minor differences: the overall range of peridotite-derived melt compositions is <0.01% different from Soderman et al. (2022), and the overall range of pyroxenite-derived melt compositions ($\Delta^{26}\mathrm{Mg}_{\mathrm{melt-source}}$) has increased by 0.04%.

We also show results using the temperature-dependent $\Delta^{26} \mathrm{Mg}_{\mathrm{olivine-melt}}$ proposed by Liu et al. (2022) for peridotite and silicadeficient pyroxenite (Fig. S6). They used olivine-glass pairs to suggest that olivine is resolvably isotopically lighter than coexisting silicate melt. As a consequence, mantle melting modelled using this constraint is predicted to generate slightly isotopically heavier equilibrium melts than by taking no olivine-melt isotopic fractionation (Fig. S6, see also Liu et al., 2023). In both lithologies, the variation in our calculated Δ^{26} Mg_{melt-source} between the two olivine-melt fractionation scenarios is small, < 0.05% over nearly all of the melting region, and similar to the typical 2 S.D. error on Mg isotope measurements of basalts (e.g., Liu et al., 2023). Given our interest in the equilibrium δ^{26} Mg variability generated by melting rather than its absolute values, and the worse fit to natural basalt data when using a non-zero olivine-melt fractionation (Liu et al., 2023), we continue with the original $\Delta^{26} Mg_{olivine-melt}$ constraint from Stracke et al. (2018).

The predicted small peridotite melting equilibrium fractionation (absolute $\Delta^{26} \rm Mg_{melt-source} < 0.05\%$, regardless of whether the olivine-melt fractionation factor is taken as zero or non-zero) is in agreement with most existing studies (Teng et al., 2007, 2010; Stracke et al., 2018). While Zhong et al. (2017) calculate that a garnet-peridotite source

could produce $\Delta^{26} \rm Mg_{melt-source}$ of magnitude 0.1‰, this large isotope fractionation can be attributed to a different choice of mineral-melt fractionation factors (e.g., a large, fixed melt-clinopyroxene Mg isotope fractionation factor, which is estimated by Zhong et al., 2017 from an isotopic offset between measured Louisville basalts and a calculated high pressure-high temperature clinopyroxene). The isotope fractionation of melts during pyroxenite partial melting is much larger than during peridotite melting, with a total range in $\Delta^{26} \rm Mg_{melt-source}$ of 0.29‰ in MIX1G (Fig. 3b). The isotopically heaviest melts ($\Delta^{26} \rm Mg_{melt-source} \approx 0.15‰)$ are produced at high pressures, and the isotopically lightest melts ($\Delta^{26} \rm Mg_{melt-source} \approx -0.10‰)$ at low pressures, in both pyroxenite lithologies considered. The potential for garnet-dominated lithologies to generate large positive Mg isotope fractionation during partial melting is consistent with Stracke et al. (2018); Liu et al. (2023).

The presence or absence of mantle minerals important for the sense of $\Delta^{26} \rm Mg_{melt-source}$ for the lithologies considered is highlighted in Fig. 3. Coloured lines show the appearance/disappearance of olivine, spinel and garnet in the mineral assemblage. In the peridotite, olivine is present over the entire melting region, whereas in both pyroxenites olivine is absent for much or all of the deep melting region (with pyroxene dominating). Garnet is present extensively at depth in both pyroxenites, with spinel appearing at lower pressures in the more MgO-rich silica-deficient pyroxenite but absent in the silica-excess pyroxenite. This contrast in mineralogy between two types of lithology, olivine-rich versus olivine-poor to olivine-free, allows us to investigate how mineralogy may directly affect $\delta^{26} \rm Mg$ of mantle melts, and contrast it to the behaviour of Fe isotopes during mantle melting discussed in Soderman et al. (2021).

We note here that we do not expect our overall conclusions about the behaviour of Mg and Fe isotope fractionation during mantle melting to be reliant on the exact topography of the mineral assemblage boundaries in P-T space or pyroxenite major-element geochemistry. This point is shown directly for Fe isotopes in Soderman et al. (2021), with similar maximum magnitude $\Delta^{57} \text{Fe}_{\text{melt-source}}$ for all three lithologies used here, despite their considerably different mineralogies. We also see similar magnitude $\Delta^{26} \text{Mg}_{\text{melt-source}}$ between the two pyroxenites in Fig. 3. For Mg isotope fractionation, the key requirements for generating extreme (either positive or negative) isotopic fractionations during melting are an olivine-poor lithology with a mineral such as spinel, garnet or clinopyroxene (all with relatively large $\Delta^{26} \text{Mg}_{\text{mineral-source}}$) in the stable mantle assemblage, to allow the isotopically extreme minerals to influence the Mg budget of the melts. Therefore, although we are referring to two specific pyroxenite models throughout this work, more gener-

ally the generation of melts with $\delta^{26} \rm Mg$ either higher or lower than that of the bulk lithology can be a consequence of melting in an olivine-poor (hence pyroxene-dominated) assemblage. We take the estimates of the maximum magnitude of these isotopic fractionations during mantle melting calculated here to be indicative of the maximum fractionations for similar sorts of olivine-poor lithologies, even if the exact pressures and temperatures of (e.g.) garnet stability are different among them. By contrast, a pyroxenite such as the aluminium-poor (and therefore garnet-poor, olivine-rich) KG1 composition that may represent an enriched source lithology in Iceland (Shorttle and Maclennan, 2011, and references therein) would generate melts with less Mg isotope variability than the MIX1G and G2 compositions used here.

3.2. Iron and magnesium isotope data

The full major, trace element, radiogenic and stable isotope data collected in this study is given in Data S1-S3 and summarised in Figs. 6, S1 & S7–9. The δ^{57} Fe of the Cook-Austral samples (Rarotonga, Aitutaki) range from 0.19-0.26% (Fig. S1), with typical 2 S.E. on multiple measurements of the same sample of \pm 0.02\%. The isotopic compositions of the two islands overlap, but Rarotonga records the lowest δ^{57} Fe, and Aitutaki the highest. The Tahaa samples have slightly lower average δ^{57} Fe than the Cook-Austral samples, from 0.17–0.20%. These OIB samples record δ^{57} Fe within the range of those measured for other Pacific OIB including Pitcairn (Nebel et al., 2019; Shi et al., 2022) and existing Society and Cook-Austral data (Teng et al., 2013). Our new Society and Rarotonga data also overlap with measured Samoan shield lavas (Soderman et al., 2021; Wang et al., 2021a), whereas Aitutaki basalts extend to slightly higher values (Fig. S7). The MORB sample S18 60/1 has the lowest δ^{57} Fe of samples measured here, $0.11\% \pm 0.01$ (2 S.E.), which is slightly lower than average MORB (Teng et al., 2013; Sossi et al., 2016), but is within 2 S.D. error of compiled global data (Fig. S1). There is no correlation between δ^{57} Fe and whole rock MgO or tracers of seawater alteration (e.g., Ba/Rb; Konter et al., 2016; Figs.

Nine of the samples were also measured for δ^{26} Mg (sample numbers limited by laboratory constraints). Rarotonga basalts have δ^{26} Mg between -0.17 and -0.27% (typical 2 S.E. \pm 0.03‰), and Aitutaki basalts are isotopically lighter, with δ^{26} Mg between -0.27 and -0.36%. The Rarotonga basalts measured here have generally higher δ^{26} Mg than existing data for Rarotonga (Fig. S7; Wang et al., 2018), and are similar to some of the highest MORB and OIB (Hawai'i) in the literature (Teng et al., 2010). The Tahaa basalt measured for δ^{26} Mg and the MORB S18 60/1 both have low δ^{26} Mg similar to the lightest Aitutaki compositions, and are also similar to the lowest δ^{26} Mg so far recorded from Society (Teng et al., 2010). The MORB sample S18 60/1 has significantly lower δ^{26} Mg than average MORB, and is the isotopically lightest (unaltered) MORB sample in the global dataset (Figs. 4, S1). There is no correlation between δ^{26} Mg and whole rock MgO or tracers of alteration (Figs. S7–S8).

3.2.1. Correction for fractional crystallisation

Fractional crystallisation drives the δ^{57} Fe of evolved melts to higher values (e.g., Teng et al., 2008; McCoy-West et al., 2018; Williams et al., 2018) due to the removal of low δ^{57} Fe phases (e.g., olivine and pyroxene, both isotopically light relative to melt). Therefore, we correct our measured δ^{57} Fe for fractional crystallisation (following Sossi et al., 2016; Nebel et al., 2019, details in Supplementary Material). Although no significant δ^{57} Fe–MgO correlation is seen in our data (Fig. S7), the MgO range of our samples is relatively narrow (7.2–12.2 wt%, plus one high MgO sample, 16.9 wt%) and the number of samples from each locality small. The fractional crystallisation corrections are small (Δ^{57} Fe < 0.01‰) for all but one sample (sample RAR-B-16, with the lowest MgO), less than the internal precision of sample analyses. For the high MgO sample RAR-B-9, which has likely undergone some crystal accumulation, we do not perform a fractional crystallisation correction (see

Supplementary Material). All previously published Fe isotope data discussed in this study (which only includes samples with 16 > MgO (wt%) > 7) have also undergone the same fractional crystallisation correction as described above.

Fractional crystallisation may affect Mg isotope compositions of basalts, although there are contrasting literature results. Some studies have found no resolvable effect on basalt $\delta^{26} Mg$ during fractional crystallisation even to low MgO values (Teng et al., 2007, 2010), whereas others have shown the effect of late-stage high $\delta^{26} \mathrm{Mg}$ Fe-Ti oxide crystallisation (Wang et al., 2018; Su et al., 2019). Although many studies have suggested there is no resolvable equilibrium $\Delta^{26} Mg_{olivine-melt}$ (e.g., Teng et al., 2007, 2010; Stracke et al., 2018), Liu et al. (2022) suggest a significant olivine-melt fractionation from measurements of olivine-glass pairs, with melt enriched in ²⁶Mg, and use this fractionation to explain high $\delta^{26} \mathrm{Mg}$ recorded in some arc lavas. However, in their basalt samples, there is no systematic resolvable change in δ^{26} Mg for samples with $\gtrsim 8$ wt% MgO. Therefore, given the high MgO nature of the samples selected here and the lack of any δ^{26} Mg-MgO correlation in our sample set (Fig. S7), we do not correct our Mg isotope data for fractional crystallisation of olivine (or oxides). This approach is also consistent with using no Mg isotope olivine-melt fractionation in our main melting model.

4. Discussion

4.1. Iron and magnesium isotopes as tracers of source and equilibrium melting process

Our model results show that Fe and Mg isotopes in melts respond differently to the presence of recycled crust in the mantle. We find that $\Delta^{26} Mg_{melt-source}$ is sensitive to the mineralogy of the mantle source, considerably more sensitive than Fe isotopes. For example, a garnetbearing mantle assemblage can have a significant impact on melt δ^{26} Mg, due to the large Δ^{26} Mg_{garnet-melt} (originating from weak garnet Mg-O bonds) and garnet's relatively high Mg content (e.g., over 50% of the total MgO budget of the melting MIX1G pyroxenite at low melt fractions and high pressure, calculated from the phase equilibria results). Therefore, changing the temperature and pressure of melting, hence the proportion of garnet present in the mantle, can have a big influence on $\Delta^{26} Mg_{melt-source}$, > 0.1% (e.g., Fig. 3b). In the pyroxenite melting models, the positive $\Delta^{26} Mg_{melt-source}$ at high pressure ($\gtrsim 20$ kbar) reflects the abundance of low $\delta^{26} \mathrm{Mg}$ pyrope (Mg-Al)-grossular (Ca-Al) garnet in the source (e.g., $\sim 55\%$ and $\sim 30\%$ adjacent to the solidus at 40 kbar in MIX1G and G2 respectively). A similar effect is seen in peridotite melting, though olivine (with a small/zero $\Delta^{26} Mg_{olivine-melt})$ dominates the Mg budget, limiting the influence of garnet on the bulk $\Delta^{26} \text{Mg}_{\text{melt}-\text{source}}$ and meaning the melts reach less extreme isotope compositions. That Mg isotopes in basalts are sensitive to the presence of garnet in their mantle source is in agreement with prior work (Huang et al., 2013; Zhong et al., 2017; Stracke et al., 2018; Wang et al., 2023).

Where spinel and/or clinopyroxene dominate the Mg budget over garnet in the mantle (both with stronger Mg-O bonds than olivine or garnet, considerably so for spinel), an opposite sense of Δ^{26} Mg_{melt-source} is predicted. In our MIX1G pyroxenite melting model, the negative $\Delta^{26} Mg_{melt-source}$ at lower pressures reflects the appearance of high δ^{26} Mg, relatively Mg-rich spinel in the residual assemblage (Fig. S4; >15% of the total MgO in the system at low melt fractions). Clinopyroxene is also present in the low pressure MIX1G residual assemblage, but because of its weaker Mg-O bonds relative to spinel has less extreme δ^{26} Mg. In the G2 pyroxenite, where spinel is absent at low pressures, isotopically heavy clinopyroxene is instead the solid phase dominating the Mg budget and results in correspondingly low δ^{26} Mg melts (Fig. S5). The extreme ranges in melt δ^{26} Mg occur where there is an olivine-poor assemblage, which would usually dominate the Mg budget and has an isotopic composition similar to, or equal, to that of silicate melt. Therefore, an olivine-poor mantle lithology containing an isotopically extreme mineral such as spinel or garnet, or clinopyroxene where the other two are absent, is capable of generating large magnitude $\Delta^{26} M g_{melt-source}$ (> 0.1%).

By contrast, melt δ^{57} Fe shows only subtle changes where garnet versus spinel and/or clinopyroxene is present in the pyroxenite assemblage (e.g., Fig. 5 in Soderman et al., 2022), because garnet contains little Fe. There is no resolvable Δ^{57} Fe_{melt-source} difference from peridotite and pyroxenite melting. Instead, Δ^{57} Fe_{melt-source} is much more strongly affected by melting degree than mantle mineralogy, largely because of the relative incompatibility of higher δ^{57} Fe Fe³⁺ than lower δ^{57} Fe Fe²⁺ during mantle melting (Dauphas et al., 2014).

The $\delta^{26}{\rm Mg}$ and $\delta^{57}{\rm Fe}$ of pyroxenite-derived melts will also depend on the bulk pyroxenite isotope composition, not just $\Delta_{\rm melt-source}$. Given the proposed origin of pyroxenite lithologies as recycled oceanic crust, or reaction hybrids between oceanic crust and peridotite and/or their melts (e.g., Sobolev et al., 2007; Herzberg, 2011), an estimate of the bulk $\delta^{26}{\rm Mg}$ and $\delta^{57}{\rm Fe}$ of mantle pyroxenite can be made from average MORB values. In the case of $\delta^{26}{\rm Mg}$, most MORB are isotopically indistinguishable from the proposed bulk silicate Earth (BSE) value/peridotites, with $\delta^{26}{\rm Mg}_{\rm average\ MORB} = -0.25 \pm 0.06\%$ and $\delta^{26}{\rm Mg}_{\rm BSE} = -0.25 \pm 0.04\%$ (Teng et al., 2010; Stracke et al., 2018; Liu et al., 2023). This similarity is the strongest argument for minimal Mg isotope fractionation during melting and fractional crystallisation of olivine \pm pyroxene (e.g., Teng et al., 2010).

The difference between $\delta^{57} \mathrm{Fe}_{\mathrm{average\ MORB}}$ and $\delta^{57} \mathrm{Fe}_{\mathrm{BSE}}$ is much greater than for Mg isotopes. Recent estimates of upper mantle/BSE compositions are 0.02-0.05\% (Sossi et al., 2016; Johnson et al., 2020), whereas estimates of average global MORB are $\approx 0.15\%$ (e.g., Teng et al., 2013; Sossi et al., 2016). Some enriched MORB record even higher $\delta^{57} Fe.$ The $\delta^{57} Fe$ offset of MORB from BSE can be mostly explained by partial melting and fractional crystallisation (Sossi et al., 2016), but recent work has highlighted the potential for source metasomatism and heterogeneity to contribute to δ^{57} Fe diversity in ridge basalts (e.g., Sun et al., 2020; Guo et al., 2023). As a result of the $\geq 0.10\%$ δ^{57} Fe difference between peridotite and oceanic crust, Fe isotopes have the potential to be a sensitive tracer to the proportion of recycled crust in the mantle source of an oceanic basalt (e.g., Nebel et al., 2019; Gleeson et al., 2020; Soderman et al., 2022, 2023). The ability of processes such as alteration and dehydration of subducted oceanic slabs to alter the bulk δ^{57} Fe of pyroxenite away from that of average global MORB remains unclear but is likely to be small (Soderman et al., 2021, 2022). However, there is considerable variability in MORB δ^{57} Fe even on a ridge-by-ridge basis (e.g., the Mid-Atlantic Ridge has an average δ^{57} Fe = 0.20 \pm 0.07\% (1\sigma) versus the East Pacific Rise with average δ^{57} Fe = $0.14 \pm 0.05\%$ (1 σ); Teng et al., 2013; Sun et al., 2020). This variation means that the bulk δ^{57} Fe of pyroxenite derived from subducted MORB could be variable regardless of whether we fully understand its origin, and is an important parameter when considering the Fe isotope signature of recycled oceanic crust in the mantle.

Given the different sensitivities of Fe-Mg isotopes to recycled crust in the mantle, in Fig. 4 we show how a combined isotope approach may be able to place unique constraints on the processes and mantle sources involved in basalt petrogenesis. To highlight the sensitivity of the isotope systems to melting in mineralogically-distinct fields of the mantle, we show the endmember MIX1G pyroxenite- and peridotitederived melts for three melting scenarios (melts generated along peridotite isentropes for potential temperature (T_n) = 1300 °C, 1400 °C and 1530 °C; see Soderman et al., 2022 for the isentropic paths). These scenarios intersect spinel-, clinopyroxene- and garnet-bearing regions of the olivine-poor pyroxenite. For each temperature scenario we show the range in melt $\delta^{57} {\rm Fe-} \delta^{26} {\rm Mg}$ along the melting paths, which include peridotite- and pyroxenite-derived melts generated from 5 kbar (in the coolest scenario) to 40 kbar (for the hottest scenario). In the coolest melting scenario for this pyroxenite composition, pyroxenite-derived melts at < 15 kbar are generated in the spinel-only (plus clinopyroxene) mantle stability field, whereas deeper melts are generated in the

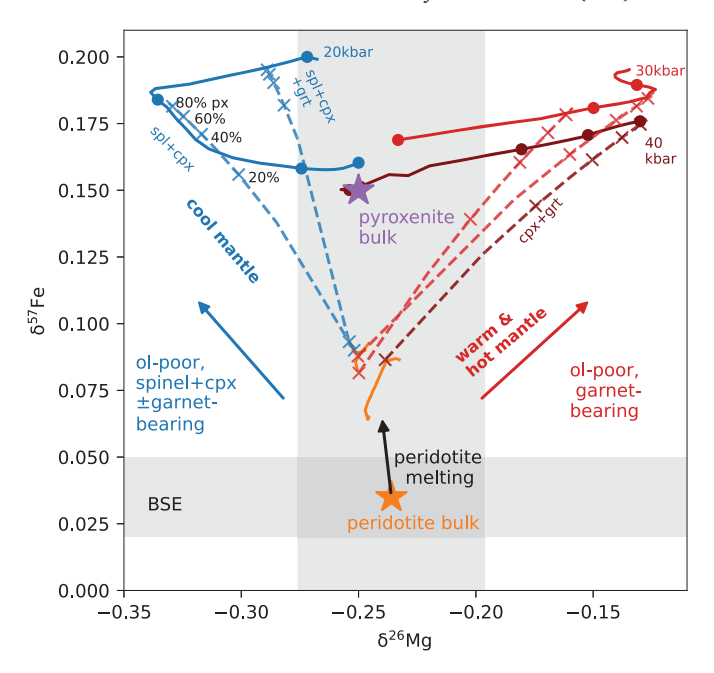


Fig. 4. Modelled $\delta^{57} {\rm Fe}$ and $\delta^{26} {\rm Mg}$ behaviour for mixing peridotite- and MIX1G-pyroxenite-derived melts. Representative peridotite and pyroxenite bulk isotope compositions shown as stars; pyroxenite bulk is taken as average global MORB (Sossi et al., 2016). Grey bars show BSE \pm typical quoted 2 S.D. uncertainty (Johnson et al., 2020; Liu et al., 2023). Melt compositions are shown for three different temperature scenarios (melting along peridotite isentropes in a 'cool' mantle (blue), $T_p = 1300$ °C, a 'warm' mantle $T_p = 1400$ °C (red), and a 'hot' mantle $T_p = 1530^{\circ}$ C (dark red); see Soderman et al., 2022). The solid lines show the isotope composition of pure pyroxenite-derived (blue, red, dark red) and peridotite-derived (orange) melts along these isentropes, with filled circles marking every 5 kbar step in pressure of melting for the pyroxenitederived melts and the deepest melting pressure (to the nearest 5 kbar) labelled. Warm and hot mantle scenarios cut off melting at < 20 kbar to be more representative of melting depth in these tectonic settings (e.g. plumes). The dashed lines show example mixing curves for increasing proportion of pyroxenite in the solid mantle, with crosses showing 20% steps in the solid fraction of pyroxenite. The mixing lines are calculated for combined melts generated given a certain lithospheric cap on the melting region (see example calculation in Soderman et al., 2022), where the average pyroxenite melting pressure will be deeper than the average peridotite melting pressure for the same mantle potential temperature due to the deeper onset of pyroxenite melting. The examples shown are for a lithospheric thickness of 15 and 45 km ($T_p = 1300$ °C), 15 and 60 km ($T_p = 1300$ °C) 1400°C) and 90 km ($T_p = 1530$ °C).

spinel-clinopyroxene-garnet stability field (Fig. 3). In the $T_p = 1400$ °C scenario, melts are generated from a garnet-bearing assemblage deeper than ~ 20 kbar, and in the $T_n = 1530$ °C scenario from deeper than ~ 25 kbar. Example mixing curves between the peridotite- and pyroxenite-derived melts in each temperature scenario are shown as dashed lines (with melts from each lithology generated along the same adiabatic path). In these mixing scenarios, melt productivity of each lithology along the relevant adiabat for a given cap on the melting region is taken from phase equilibria results in Soderman et al. (2022), allowing for the mixing calculations to be recast in terms of solid pyroxenite fraction in the source (rather than pyroxenite-derived melt fraction) along the curves – see caption of Fig. 4 for more details. We note that we are not choosing specific temperatures or melting depths with the aim of putting particular depth or temperature constraints on the mantle source of oceanic basalts, as these numbers would trade-off with the pyroxenite bulk major element (see, e.g., results for G2 pyroxenite in Fig. 3) and Fe-Mg isotope composition. Instead, the temperatures and depths are chosen to highlight the range of Fe-Mg melt isotope compositions predicted by our model, given the underlying assumption of an olivine-poor recycled crust lithology as a mantle component.

Any mantle component with higher δ^{57} Fe than BSE, which can include pyroxenite, will produce melts with higher δ^{57} Fe than pure peridotite-derived melts, since the partial melting fractionation is largely independent of mineralogy. The example of bulk pyroxenite δ^{57} Fe equal to average global MORB is shown in Fig. 4. Ultimately, the majority of oceanic basalt δ^{57} Fe variation will be controlled by the bulk isotope composition of the source (Soderman et al., 2021, 2023) because $\Delta^{57} Fe_{melt-source}$ is small (< 0.07‰, even for melt fractions < 0.5%). Magnesium isotopes can place constraints on the appearance of residual garnet in the mantle source (hence melting depth, related to temperature and lithology). Melts from a mantle source with significant garnet but minimal olivine, such as the pyroxenites used here at high pressure, will therefore produce a positive trend in Fe-Mg isotope space when mixed with peridotite-derived melts. By contrast, an input from a garnet-olivine-poor, spinel-and/or clinopyroxene-bearing melt source region produces negative slopes depending on the proportion of isotopically heavy clinopyroxene and spinel. The switch between these scenarios could be achieved through varying mantle T_p , final melting depth (hence lithospheric thickness) and/or source mineralogy. At high mantle T_p for example, large pyroxenite $\Delta^{26} Mg_{melt-source}$ reduces to zero as the pyroxenite melt fraction increases with decompression. In a melting region where spinel, garnet and clinopyroxene are present, such as the near-solidus assemblage from 15-25 kbar in our modelled MIX1G pyroxenite, $\Delta^{26} Mg_{melt-source}$ swings from positive to negative reflecting the change from a garnet-pyroxene to spinel-pyroxene-dominated melting residue. This evolution in melt composition towards less negative $\Delta^{26} Mg_{melt-source}$ as the Mg budget of a melting pyroxenite switches from being garnet-dominated to clinopyroxene-dominated is consistent with the fractional melting model of G2 pyroxenite from Stracke et al. (2018).

Magnesium and Fe isotopes therefore provide complementary perspectives on the petrogenesis of oceanic basalts, making their combination a powerful tool. Both systems can track the proportion of recycled crust versus peridotite contributing to melt production. The Mg isotope composition of oceanic basalts can directly track source mineralogy (linked to depth of melting and/or type of pyroxenite). The δ^{57} Fe of the basalts additionally reflects the δ^{57} Fe value of the mantle source (both peridotite and pyroxenite components), which record past processes such as low temperature or hydrothermal alteration of crust prior to subduction (see Soderman et al., 2021 for summary), or metasomatism of the sub-oceanic lithospheric mantle (e.g., Weyer and Ionov, 2007; Konter et al., 2016; Sun et al., 2020). These processes may be non-unique for generating high δ^{57} Fe basalts (Soderman et al., 2021). Because both Fe and Mg are major elements in the mantle, the isotopic signal of recycled crustal melts does not overwhelm the isotopic signature of peridotite melts, unlike incompatible trace elements.

4.2. Explaining the global Fe-Mg isotope variation in oceanic basalts

Our model results can explain why nearly all published δ^{57} Fe in primitive oceanic basalts (MORB and OIB), with minimal trace element evidence for carbonate in their source, are higher than BSE, but δ^{26} Mg of similarly-filtered oceanic basalts scatter to either side (Fig. 1). Our model predicts that most oceanic basalts will have higher δ^{57} Fe than peridotite for two reasons. First, because mantle melting produces small, but potentially resolvable, positive Δ^{57} Fe_{melt-source}, especially at very low melt fractions. Second, because of the importance of bulk source isotope composition on controlling $\delta^{\rm 57}{\rm Fe}$ of mantle melts, and the expectation that mantle source enrichment through metasomatism or recycled crustal input should increase the δ^{57} Fe of the source relative to peridotite. The range of isotopic compositions that can be generated in this way could be large. By contrast, the mantle source $\delta^{26} Mg$ is unlikely to vary substantially (e.g., the similarity of δ^{26} Mg of mean MORB and BSE; Teng et al., 2010), and therefore variability in δ^{26} Mg of oceanic basalts is more likely related to process (e.g., depth of melting). Partial melting can generate > 0.2% difference in $\Delta^{26} \mathrm{Mg}_{\mathrm{melt-source}}$ (\approx -0.1 to +0.1) from the same mixed peridotite-pyroxenite mantle, depending on the specific mineralogy in the melting region.

4.2.1. Fe-Mg isotopes in MORB

Our predicted behaviour of melt $\delta^{26}{\rm Mg}$ produced at different melting depths is consistent with the variation in MORB $\delta^{26}{\rm Mg}$ from the Mid-Atlantic Ridge (Fig. 5). MORB from shallow ridge segments (indicating relatively high, and therefore deep, melt production, perhaps due to relatively high mantle potential temperature; Klein and Langmuir, 1987) have higher $\delta^{26}{\rm Mg}$ than those from deeper ridge segments. This result is consistent with relatively high $\delta^{26}{\rm Mg}$ melts being derived from the garnet stability field where melting starts deep, compared to low $\delta^{26}{\rm Mg}$ generated when melting is dominated by shallow, spinel-pyroxene melting.

For the melting scenarios shown in Figs. 4,5, < 10% silica-deficient pyroxenite is required in the mantle source to generate most of the $\delta^{26} \mathrm{Mg}$ range of the Mid-Atlantic Ridge basalts. The shallowest and deepest ridge samples require up to 20% solid pyroxenite (given the error on $\delta^{26} Mg$ measurements; the upper end of this range may be unrealistic globally but could be sampled on a local scale). Estimates of < 10% solid pyroxenite are consistent with existing estimates of the global MORB source (e.g., Hirschmann and Stolper, 1996). The exact proportion of pyroxenite required would vary based on the T_n and type of pyroxenite chosen, but we use the scenario shown here to highlight the range of melt δ^{26} Mg that could be produced with small amounts of pyroxenite in the MORB-source mantle. These estimates of pyroxenite fraction in the MORB source also match with Fe isotope data, where modelled peridotite-derived melts by themselves cannot generate the Fe isotope variability seen in global MORB (Figs. 1, S1, Soderman et al., 2022). We note that the MORB S18 60/1 measured here, unique amongst other MORB for its extreme radiogenic isotope composition (Kamenetsky et al., 2001), has a low δ^{26} Mg that would require significant pyroxenite fraction not matched by its relatively low δ^{57} Fe (similar to the Louisville OIBs; Fig. 7). Additional processes not considered by this model (see section 4.3) may be relevant to these samples.

4.2.2. Fe-Mg isotopes in Pacific plume-related basalts

Ocean island volcanoes and seamounts in the south Pacific including Pitcairn, the Societies, Samoa, Louisville and the Cook-Austral islands are thought to be formed by melting mantle plumes containing recycled oceanic and/or continental crust material (e.g., Zindler and Hart, 1986; Woodhead and Devey, 1993; Hofmann, 1997; Eisele et al., 2002; Workman et al., 2004; Willbold and Stracke, 2006; Jackson et al., 2007; Jackson and Dasgupta, 2008; Stracke, 2012). These volcanoes produce basalts with distinct radiogenic isotope compositions both between and within individual plumes (Fig. 6).

While major elements in basalts and trace elements in olivine have been used previously to identify links between mantle lithologies and radiogenic isotope endmembers in OIB (e.g., Sobolev et al., 2005; Jackson and Dasgupta, 2008), more recently Fe and Mg stable isotopes have also been used to this end, particularly for Pacific volcanoes. For example, Konter et al. (2016) attribute high δ^{57} Fe (> 0.4‰) in rejuvenated Samoan basalts to combinations of partial melting, an offset of the isotopic composition of the mantle source from ambient mantle due to pyroxenite, and fractional crystallisation. Pitcairn basalts record the next highest δ^{57} Fe in the Pacific volcanoes, attributed to a high δ^{57} Fe mantle pyroxenite component (~ 0.3%) produced by low-degree melting of subducted eclogite, which also hosts the EM1 radiogenic isotope signature (Nebel et al., 2019). The combination of high δ^{57} Fe with low $\delta^{26} \mathrm{Mg}$ has additionally been used to suggest an eclogitic mantle component containing carbonate (dolomite)-bearing sediment (Wang et al., 2018; Shi et al., 2022) in the Pitcairn mantle source.

Our new data continues the pattern seen in global oceanic basalts, where δ^{57} Fe are higher than BSE estimates, whereas δ^{26} Mg scatter either side. From our data, Cook-Austral basalts are similar to Pitcairn basalts in Fe–Sr isotope space, but are offset in Fe–Pb isotope space

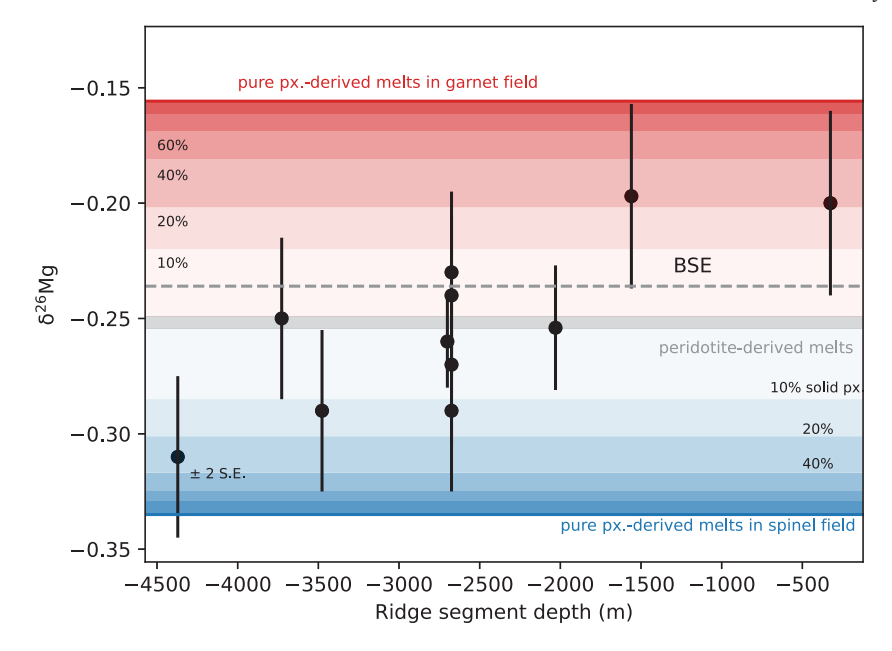


Fig. 5. Published δ^{26} Mg for Mid-Atlantic Ridge MORB vs ridge segment depth. Peridotite- and MIX1G pyroxenite (px)-derived melts as in Fig. 4, but showing only the endmember average melt compositions generated along the complete isentrope (i.e. minimal lithospheric cap) for $T_p = 1300$ and 1400 °C to be applicable to MORB generation. The endmember pyroxenite-derived melts are generated by melting in the spinel-bearing and garnet-bearing regions of the pyroxenite mantle lithology. Shading shows mixing between a pure peridotite and pure pyroxenite source, with intervals of 10, 20% and then subsequent 20% increments in solid pyroxenite in the source shown. The exact δ^{26} Mg of the endmember melts and the mixing proportions would change for a different set of mantle potential temperatures chosen; those shown here are one representative example from the full melting model in Fig. 3. MORB data from Teng et al. (2010), BSE from Liu et al. (2023). Ridge depth data as described in the Supplementary Material.

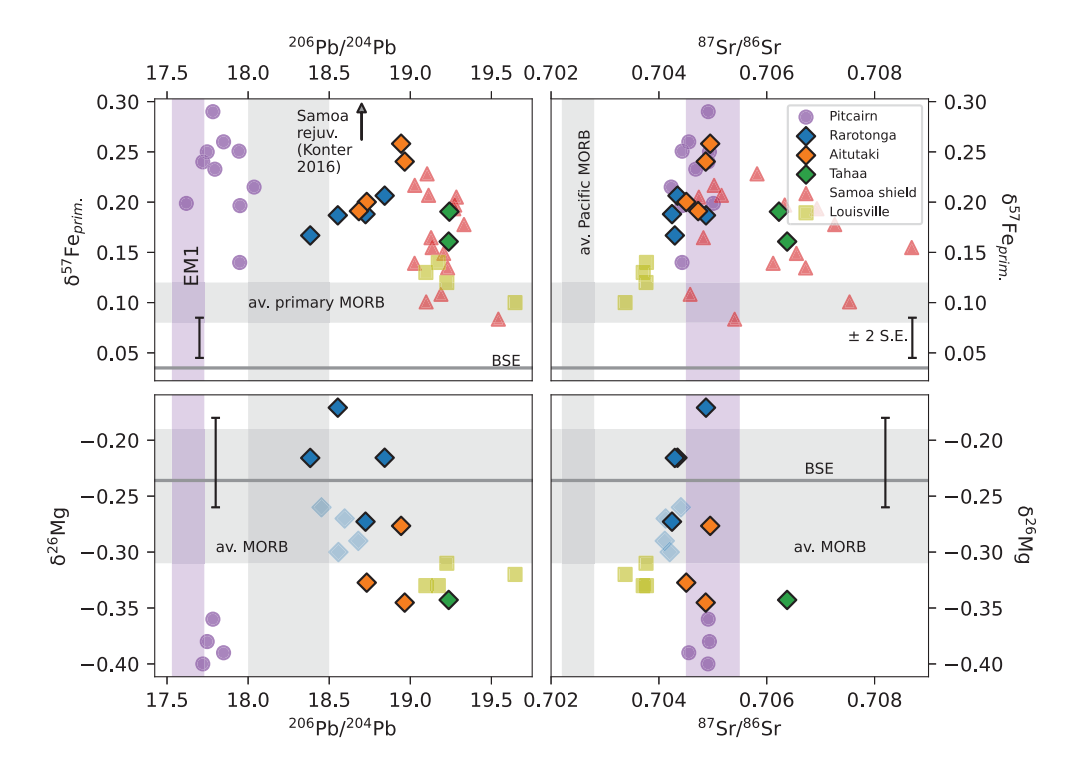


Fig. 6. Stable Fe and Mg isotope variation with radiogenic isotopes for Pacific ocean island basalts. New samples studied here shown with black outlines, typical \pm 2 S.E. errors from our measurements are also shown. Pitcairn data from Wang et al. (2018); Nebel et al. (2019); Shi et al. (2022); Louisville data from Zhong et al. (2017); Shi et al. (2022); existing Rarotonga data from Wang et al. (2018); Samoa data from Konter et al. (2016); Soderman et al. (2021); Wang et al. (2021a). All Fe isotope data is shown corrected for fractional crystallisation and only literature samples with 16 > MgO (wt %) > 7 are shown. Reference marks are shown for the EM1 endmember (Konter et al., 2008) in Sr-Pb isotope space (purple), BSE (dark grey line, Sossi et al., 2016; Johnson et al., 2020; Liu et al., 2023) and average MORB (pale grey band): for Mg from Teng et al., 2010; for Fe, primary MORB to compare to fractional crystallisation corrected data, from Sossi et al., 2016; for Sr-Pb average Pacific MORB (for comparison to Pacific OIB) from Stracke et al. (2005).

(Fig. 6) as well as in trace element ratios (Fig. S9). The Pitcairn basalts have a high δ^{57} Fe-less radiogenic Pb component (Nebel et al., 2019), whereas Rarotonga and Aitutaki basalts have similarly high maximum δ^{57} Fe, but associated with a more radiogenic Pb component (Fig. 6). The high δ^{57} Fe endmember in Pitcairn has been suggested as a reaction pyroxenite (eclogite-derived melts reacted with peridotite; Nebel et al., 2019; Shi et al., 2022). Although the exact processes that can generate a pyroxenite/eclogite with such a high δ^{57} Fe remain unclear (Soderman et al., 2021, 2022), a similar isotope composition linked to recycled crust has also been suggested for Galápagos spreading ridge basalts (Gleeson et al., 2020). While the Cook-Austral samples shown here mostly do not record as high δ^{57} Fe as Pitcairn, they are still higher than can be explained by melting of ambient (BSE-like) peridotite mantle. The Aitutaki basalts have lower δ^{26} Mg than the Rarotonga basalts, and the Cook-Austral samples overall have high Sm/Yb (Fig. S9) likely linked to low degrees of melting beneath thick lithosphere (Dasgupta et al., 2010) and contributing to their relatively high δ^{57} Fe.

Given the high δ^{57} Fe and variable δ^{26} Mg measured in the Cook-Austral and Society basalts, our new data supports the presence of recycled crustal component(s) in the mantle source of south Pacific plume-related basalts, as suggested by their radiogenic isotope compositions. We note that mixing between an isotopically extreme pyroxenitederived melt (e.g., high or low $^{206}\text{Pb}/^{204}\text{Pb}$, high $\delta^{57}\text{Fe}$) and a depleted mantle melt (intermediate 206 Pb/ 204 Pb, low δ^{57} Fe) may not be expected to generate any significant correlation between Fe-Pb isotopes (Gleeson et al., 2020) because of the large disparity in Pb concentrations between the pyroxenite- and peridotite-derived melts, compared to similar Fe (or Mg) concentrations. Additionally, high δ^{57} Fe and extreme radiogenic isotope compositions (e.g. high ⁸⁷Sr/⁸⁶Sr) are likely associated with different parts of recycled material (bulk crust versus specific sediments respectively). These considerations mean it may be easy to decouple major element isotope from trace element isotope behaviour, which can make linking the geochemical histories from the two approaches difficult, although Fe-radiogenic isotope correlations are seen in some plume settings (e.g., Nebel et al., 2019; Soderman et al., 2021).

4.3. Are alternative mantle sources or processes required to generate global oceanic basalt Fe-Mg isotope variability?

Coupling the Fe-Mg isotope data with our model results for bilithologic mantle melting, much of the variation in global primitive basalt Fe-Mg isotope ratios can be explained by varying amounts of melts (with equilibrium isotope fractionation) derived from recycled oceanic crustal sources with high δ^{57} Fe, and variable δ^{26} Mg as a consequence of melt forming at variable pressures and temperatures (Figs. 7, S1). We show mixed peridotite-pyroxenite-derived melts for two different bulk pyroxenite δ^{57} Fe values (average MORB and the proposed pyroxenite endmember in the Pitcairn plume; Nebel et al., 2019). We have shown the full range of mixed peridotite-pyroxenite-derived melts (i.e., 0–100% solid pyroxenite) to highlight theoretical melt variability relative to empirical data, but note that large solid pyroxenite fractions globally in the mantle are unlikely to be realistic, even though high pyroxenite-derived melt fractions can be sampled on a local scale.

With the Pitcairn-like δ^{57} Fe, much of the Pacific OIB basalt Fe-Mg isotope data, including from Hawai'i, Society and the Cook-Austral islands, would be matched by moderate amounts of recycled crust in the source, < 10% for Hawaiian basalts and < 20% for others, approaching the pyroxenite limit expected for a buoyant, hot mantle plume when considering harzburgite as an important mantle lithology (Shorttle et al., 2014). In the Hawaiian dataset, nearly all Fe-Mg isotope variability (with the exception of a high δ^{57} Fe outlier, and the two lowest δ^{57} Fe- δ^{26} Mg basalts) could be generated within error by an approximately constant source pyroxenite fraction and varying melting degrees with $T_p = 1530$ °C (alongside other non-unique solutions). However, these conclusions rely on 1) the existence of some mantle pyroxenite with bulk δ^{57} Fe significantly higher than average MORB (otherwise

the widespread solid pyroxenite fractions required sometimes become implausibly high), and 2) the generation of some low $\delta^{26} \rm Mg$ oceanic basalts from a non garnet-dominated mantle source (e.g. the Aitutaki basalts studied here).

On point 1), studies have either identified or implied the presence of mantle and lithospheric domains with such high bulk δ^{57} Fe in both OIB and MORB sources (Williams and Bizimis, 2014; Nebel et al., 2019; Gleeson et al., 2020; Sun et al., 2020; Guo et al., 2023), even if the processes that occur to create such widespread variation in bulk δ^{57} Fe of pyroxenite remain unidentified (Soderman et al., 2021, 2022). On point 2), melts generated from a garnet-free pyroxenite assemblage may be applicable for contributing to MORB, but are unrealistically shallow for melting beneath thick lithosphere in many plume settings, including the Cook-Austral islands studied here (Dasgupta et al., 2010). While much of the range of melts with negative $\Delta^{26} M g_{melt-source}$ in Fig. 7 is generated from a deeper spinel + pyroxene + garnet-bearing assemblage rather than a completely garnet-free one which may be applicable in some settings, it is overall more difficult to identify plausible melting conditions for OIB (hot mantle, relatively deep melting) that generate large negative $\Delta^{26} \mathrm{Mg}_{\mathrm{melt-source}}$ than positive. For example, Pitcairn basalts have a lower $\delta^{26} Mg$ than our model can produce (even with 100% of pyroxenite-derived melt) without offsetting the bulk pyroxenite δ^{26} Mg away from that of BSE and average MORB. More broadly, the global basalt datasets also show variability beyond that predicted by our equilibrium fractionation model. Consequently, there are several categories of alternative sources and/or processes that the more extreme cases may point to:

- 1. Pyroxenite with a non-MORB-like composition in both, or sometimes only one of, $\delta^{26}{\rm Mg}$ and $\delta^{57}{\rm Fe}.$ As discussed above, it is not yet clear exactly what processes acting between oceanic crust generation at a mid-ocean ridge and eventual melting as a pyroxenite component in the mantle could generate widespread, variable heterogeneity in bulk pyroxenite isotope composition. Source metasomatism (i.e. forming crustal pyroxenites) by low-degree melts may be important.
- 2. Exotic mantle source components, especially recycled carbonate for the generation of low $\delta^{26} \mathrm{Mg}$ basalts, such as the 'ghost' Mg-rich carbonate with a very specific origin proposed in Pitcairn (Wang et al., 2018). We note that significant Mg component in carbonate (and/or a large volume of subducted carbonate) would be needed to affect the bulk $\delta^{26}{\rm Mg}$ of the mantle source, which may limit the widespread impact on $\delta^{26} Mg$ of oceanic basalts. If calcite (typically 0.8 wt% MgO, δ^{26} Mg $\geq -5\%$; Wang et al., 2018) dominates the subducted carbonate, 15% carbonate in a peridotite mantle $(39.5 \text{ wt}\% \text{ MgO}, \delta^{26} \text{Mg} = -0.24\%; \text{ Davis et al., } 2009; \text{ Liu et al., }$ 2023) would only impact the bulk source δ^{26} Mg by < 0.02‰, but we would expect to see this Ca-rich source component reflected in the major element chemistry of the melts. In Pitcairn, Wang et al. (2018) invoke a specific dolomite-dominated carbonate sediment, and propose that only the Mg isotopic signature (and not raised CaO/Al₂O₃) of the carbonate-bearing sediment is recorded in the Pitcairn basalts, potentially arising through subduction-related decarbonation processes. We note that there is no requirement from our model for most of the Pacific OIB to have such a low $\delta^{26} Mg$ component in their mantle source.
- 3. Disequilibrium isotope fractionation during diffusion (e.g. meltrock reaction during metasomatism of the lithospheric mantle, or melt percolation en route to the surface). For example, diffusive fractionation during melt migration could result in low melt δ^{26} Mg and high δ^{57} Fe (e.g., Weyer and Ionov, 2007; Liu et al., 2023). Studies have noted that negative slopes in δ^{57} Fe versus δ^{26} Mg in whole-rock basalts would be predicted for diffusive Fe-Mg exchange during melt percolation through peridotite (e.g., Liu et al., 2023). Most Fe and/or Mg isotope observational evidence for disequilibrium fractionation during melt transport or metasomatism

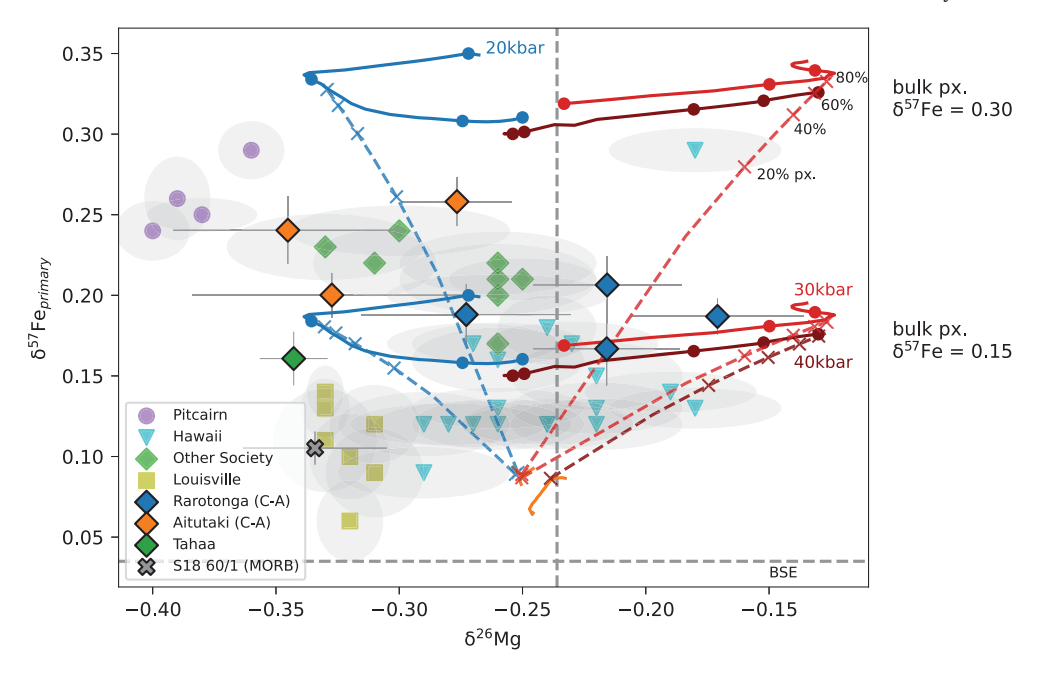


Fig. 7. Primary δ^{57} Fe vs δ^{26} Mg for our new samples (coloured, black outlines) and existing ocean island basalt data. Pyroxenite model melts shown as red and maroon ($T_p = 1400$ and 1530 °C respectively) and blue (for $T_p = 1300$ °C) lines as in Fig. 4. Orange lines are the equivalent peridotite-derived melts. Crosses on the dashed example mixing curves show 20% increments in the proportion of pyroxenite in the mantle source. Filled circles mark every 5 kbar in melting pressure for pyroxenite-derived melts, with the deepest melting pressure (to the nearest 5 kbar) labelled. The results of using two different bulk pyroxenite δ^{57} Fe values (0.15 and 0.30 ‰) are shown for each temperature scenario. Error bars on new data and error ellipses on published data are 2 S.E., literature samples filtered for those with 16 > MgO > 7 wt%. BSE values from Sossi et al. (2016); Johnson et al. (2020); Liu et al. (2023). Isotope data sources as in Fig. 6, with Hawai'i and extra Society islands data from Teng et al. (2008, 2010, 2013).

has so far been found in metasomatised peridotite (e.g., Zhao et al., 2017) or reaction-derived lithospheric mantle pyroxenites (Hu et al., 2016) rather than the subsequently erupted melts, so this process should be investigated further in the context of generating Fe-Mg isotope variability in basalts. Additionally, disequilibrium isotope fractionation has been identified in zoned crystals related to melt-crystal diffusion (e.g., Dauphas et al., 2010; McCoy-West et al., 2018) but it is unclear if this process can generate significant isotopic variability on a bulk rock scale.

5. Conclusions

With a combined mantle melting and equilibrium isotope fractionation model we show that partial melting of a mantle source containing both peridotite and recycled oceanic crust (pyroxenite) can produce melts that are all isotopically heavier than BSE in Fe isotope space, but spread either side of BSE in Mg isotope space. This predicted distribution of Fe and Mg isotope data in mantle melts is seen in the global basalt dataset for the two isotope systems. The contrasting behaviour arises because δ^{57} Fe of primitive basalts is predominantly sensitive to the bulk isotope composition of their mantle source during melting of a mixed peridotite and pyroxenite mantle. By contrast, $\delta^{26} \mathrm{Mg}$ of the same basalts is considerably more sensitive to the mineralogy (hence, for example, melting depth) of the source region. Where olivine (which would usually dominate the Mg budget of peridotite-derived melts) is only present in relatively small quantities in a mantle lithology, such as in recycled crust, the isotopically-extreme minerals garnet, spinel or pyroxene can instead dominate the Mg budget. Positive and negative $\Delta^{26} {\rm Mg_{melt-source}}$ can then be generated, meaning that low $\delta^{26} {\rm Mg}$ mantle components such as carbonate may not need to be invoked. However, additional processes operating to fractionate Fe and Mg isotopes, such as disequilibrium fractionation, may be required for the generation of more extreme low δ^{26} Mg and/or high δ^{57} Fe basalts. Both Fe and Mg isotopes may individually be able to trace the proportion of recycled crust in the mantle source, but together can give complementary information on the mantle source and petrogenetic history of basalts.

CRediT authorship contribution statement

Caroline R. Soderman: Writing – review & editing, Writing – original draft, Methodology, Investigation, Conceptualization. Simon Matthews: Writing – review & editing, Writing – original draft, Methodology. Oliver Shorttle: Writing – review & editing, Writing – original draft, Supervision. Matthew G. Jackson: Writing – review & editing, Investigation, Conceptualization. James M.D. Day: Writing – review & editing, Investigation. Vadim Kamenetsky: Writing – review & editing. Helen M. Williams: Writing – review & editing, Writing – original draft, Supervision, Methodology, Investigation, Conceptualization.

Declaration of competing interest

The authors declare that they have no known competing financial interests or personal relationships that could have appeared to influence the work reported in this paper.

Data availability

Data is available in the Supplementary Materials.

Acknowledgements

We are grateful to Andreas Stracke and an anonymous reviewer for their comments which greatly improved this manuscript, and Rosemary Hickey-Vargas for editorial handling. We thank Ed Tipper for support with Mg isotope purification and mass spectrometry, Marie-Laure Bagard for support with Fe isotope mass spectrometry, and Michael Bizimis for the radiogenic isotope analytical effort. CRS would also like to thank Angus Rogers for useful discussions about Aitutaki. Hand specimens of samples RAR-B-1, -9, and -12 were provided by the Department

of Mineral Sciences, Smithsonian Institution. For the purpose of open access, the author has applied a Creative Commons Attribution (CC BY) licence to any Author Accepted Manuscript version arising. This work was supported by Natural Environment Research Council studentship NE/L002507/1 (to CRS), UK Research and Innovation Future Leaders Fellowship grant MR/V02292X/1 (supporting CRS), Natural Environment Research Council grant NE/T012455/1 (to OS); Natural Environment Research Council grant NE/V011383/1 (to OS); NSF grant NSF-EAR-1918322 (JMDD); and NSF grant OCE-1929095 (to MGJ) which supported analysis of TAA-B-21.

Appendix A. Supplementary material

Supplementary material related to this article can be found online at https://doi.org/10.1016/j.epsl.2024.118749.

References

- Allègre, C.J., Turcotte, D.L., 1986. Implications of a two-component marble-cake mantle. Nature 323 (6084), 123–127.
- Chauvel, C., Hofmann, A.W., Vidal, P., 1992. HIMU-EM: the French Polynesian connection. Earth Planet. Sci. Lett. 110 (1-4), 99-119.
- Chauvel, C., McDonough, W., Guille, G., Maury, R., Duncan, R., 1997. Contrasting old and young volcanism in Rurutu Island, Austral chain. Chem. Geol. 139 (1–4), 125–143.
- Dasgupta, R., Jackson, M.G., Lee, C.-T.A., 2010. Major element chemistry of ocean island basalts—conditions of mantle melting and heterogeneity of mantle source. Earth Planet. Sci. Lett. 289 (3–4), 377–392.
- Dauphas, N., Teng, F.-Z., Arndt, N.T., 2010. Magnesium and iron isotopes in 2.7 Ga Alexo komatiites: mantle signatures, no evidence for Soret diffusion, and identification of diffusive transport in zoned olivine. Geochim. Cosmochim. Acta 74 (11), 3274–3291.
- Dauphas, N., Roskosz, M., Alp, E.E., Neuville, D.R., Hu, M.Y., Sio, C.K., Tissot, F.L.H., Zhao, J., Tissandier, L., Médard, E., Cordier, C., 2014. Magma redox and structural controls on iron isotope variations in Earth's mantle and crust. Earth Planet. Sci. Lett. 398, 127–140.
- Davis, F.A., Tangeman, J.A., Tenner, T.J., Hirschmann, M.M., 2009. The composition of KLB-1 peridotite. Am. Mineral. 94 (1), 176–180.
- Ding, Y., Jin, X., Li, X., Li, Z., Liu, J., Wang, H., Zhu, J., Zhu, Z., Chu, F., 2022. Magnesium isotopic composition of back-arc basin lavas and its implication for the recycling of serpentinite-derived fluids. Mar. Geol. 453, 106921.
- Eisele, J., Sharma, M., Galer, S.J., Blichert-Toft, J., Devey, C.W., Hofmann, A.W., 2002. The role of sediment recycling in EM-1 inferred from Os, Pb, Hf, Nd, Sr isotope and trace element systematics of the Pitcairn hotspot. Earth Planet. Sci. Lett. 196 (3–4), 197–212
- Gleeson, M.L.M., Gibson, S.A., Williams, H.M., 2020. Novel insights from Fe-isotopes into the lithological heterogeneity of Ocean Island Basalts and plume-influenced MORBs. Earth Planet. Sci. Lett. 535.
- Guo, P., Niu, Y., Chen, S., Duan, M., Sun, P., Chen, Y., Gong, H., Wang, X., 2023. Low-degree melt metasomatic origin of heavy Fe isotope enrichment in the MORB mantle. Earth Planet. Sci. Lett. 601, 117892.
- Hauri, E.H., Hart, S.R., 1993. Re-Os isotope systematics of HIMU and EMII oceanic island basalts from the south Pacific Ocean. Earth Planet. Sci. Lett. 114 (2–3), 353–371.
- Hauri, E.H., Hart, S.R., 1997. Rhenium abundances and systematics in oceanic basalts. Chem. Geol. 139 (1–4), 185–205.
- Herzberg, C., 2011. Identification of source lithology in the Hawaiian and Canary Islands: implications for origins. J. Petrol. 52 (1), 113–146.
- Hirschmann, M.M., Stolper, E.M., 1996. A possible role for garnet pyroxenite in the origin of the "garnet signature" in MORB. Contrib. Mineral. Petrol. 124 (2), 185–208.
- Hirschmann, M.M., Kogiso, T., Baker, M.B., Stolper, E.M., 2003. Alkalic magmas generated by partial melting of garnet pyroxenite. Geology 31 (6), 481–484.
- Hofmann, A.W., 1997. Mantle geochemistry: the message from oceanic volcanism. Nature 385 (6613), 219–229.
- Hu, Y., Teng, F.-Z., Zhang, H.-F., Xiao, Y., Su, B.-X., 2016. Metasomatism-induced mantle magnesium isotopic heterogeneity: evidence from pyroxenites. Geochim. Cosmochim. Acta 185, 88–111.
- Huang, F., Chen, L., Wu, Z., Wang, W., 2013. First-principles calculations of equilibrium Mg isotope fractionations between garnet, clinopyroxene, orthopyroxene, and olivine: implications for Mg isotope thermometry. Earth Planet. Sci. Lett. 367, 61–70.
- Huang, S., Farkaš, J., Jacobsen, S.B., 2011a. Stable calcium isotopic compositions of Hawaiian shield lavas: evidence for recycling of ancient marine carbonates into the mantle. Geochim. Cosmochim. Acta 75 (17), 4987–4997.
- Jackson, M.G., Dasgupta, R., 2008. Compositions of HIMU, EM1, and EM2 from global trends between radiogenic isotopes and major elements in ocean island basalts. Earth Planet. Sci. Lett. 276 (1–2), 175–186.
- Jackson, M.G., Hart, S.R., Koppers, A.A.P., Staudigel, H., Konter, J., Blusztajn, J., Kurz, M., Russell, J.A., 2007. The return of subducted continental crust in Samoan lavas. Nature 448 (7154), 684–687.

- Jackson, M.G., Hart, S.R., Konter, J.G., Kurz, M.D., Blusztajn, J., Farley, K.A., 2014. Helium and lead isotopes reveal the geochemical geometry of the Samoan plume. Nature 514 (7522), 355–358.
- Jackson, M.G., Halldórsson, S.A., Price, A., Kurz, M.D., Konter, J.G., Koppers, A.A.P., Day, J.M.D., 2020. Contrasting old and young volcanism from Aitutaki, Cook Islands: implications for the origins of the cook–austral volcanic chain. J. Petrol. 61 (3), egaa037.
- Johnson, C., Beard, B., Weyer, S., 2020. High-temperature Fe isotope geochemistry. In: Iron Geochemistry: An Isotopic Perspective. Springer, pp. 85–147.
- Kamenetsky, V.S., Maas, R., Sushchevskaya, N.M., Norman, M.D., Cartwright, I., Peyve, A.A., 2001. Remnants of Gondwanan continental lithosphere in oceanic upper mantle: evidence from the South Atlantic Ridge. Geology 29 (3), 243–246.
- Klein, E.M., Langmuir, C.H., 1987. Global correlations of ocean ridge basalt chemistry with axial depth and crustal thickness. J. Geophys. Res., Solid Earth 92 (B8), 8089–8115.
- Konter, J.G., Hanan, B.B., Blichert-Toft, J., Koppers, A.A.P., Plank, T., Staudigel, H., 2008.
 One hundred million years of mantle geochemical history suggest the retiring of mantle plumes is premature. Earth Planet. Sci. Lett. 275 (3–4), 285–295.
- Konter, J.G., Pietruszka, A.J., Hanan, B.B., Finlayson, V.A., Craddock, P.R., Jackson, M.G., Dauphas, N., 2016. Unusual δ^{56} Fe values in Samoan rejuvenated lavas generated in the mantle. Earth Planet. Sci. Lett. 450, 221–232. ISSN 0012821X.
- Lambart, S., Baker, M.B., Stolper, E.M., 2016. The role of pyroxenite in basalt genesis: melt-PX, a melting parameterization for mantle pyroxenites between 0.9 and 5 GPa. J. Geophys. Res., Solid Earth 121 (8), 5708–5735.
- Liu, X.-N., Hin, R.C., Coath, C.D., van Soest, M., Melekhova, E., Elliott, T., 2022. Equilibrium olivine-melt Mg isotopic fractionation explains high δ^{26} Mg values in arc lavas. Geochem. Perspect. Lett. 22, 42–47.
- Liu, X.-N., Hin, R.C., Coath, C.D., Bizimis, M., Su, L., Ionov, D.A., Takazawa, E., Brooker, R., Elliott, T., 2023. The magnesium isotopic composition of the mantle. Geochim. Cosmochim. Acta 358, 12–26.
- Macris, C.A., Manning, C.E., Young, E.D., 2015. Crystal chemical constraints on intermineral Fe isotope fractionation and implications for Fe isotope disequilibrium in San Carlos mantle xenoliths. Geochim. Cosmochim. Acta 154, 168–185.
- McCoy-West, A.J., Fitton, J.G., Pons, M.-L., Inglis, E.C., Williams, H.M., 2018. The Fe and Zn isotope composition of deep mantle source regions: insights from Baffin Island picrites. Geochim. Cosmochim. Acta 238, 542–562.
- Nebel, O., Sossi, P.A., Bénard, A., Arculus, R.J., Yaxley, G.M., Woodhead, J.D., Davies, D.R., Ruttor, S., 2019. Reconciling petrological and isotopic mixing mechanisms in the Pitcairn mantle plume using stable Fe isotopes. Earth Planet. Sci. Lett. 521, 60–67.
- Pertermann, M., Hirschmann, M.M., 2003. Partial melting experiments on a MORB-like pyroxenite between 2 and 3 GPa: constraints on the presence of pyroxenite in basalt source regions from solidus location and melting rate. J. Geophys. Res., Solid Earth 108 (B2). ISSN 01480227.
- Rose, J., Koppers, A.A.P., 2019. Simplifying age progressions within the Cook-Austral islands using ARGUS-VI high-resolution 40Ar/39Ar incremental heating ages. Geochem. Geophys. Geosyst. 20 (11), 4756–4778.
- Shi, J.-H., Zeng, G., Chen, L.-H., Hanyu, T., Wang, X.-J., Zhong, Y., Xie, L.-W., Xie, W.-L., 2022. An eclogitic component in the Pitcairn mantle plume: evidence from olivine compositions and Fe isotopes of basalts. Geochim. Cosmochim. Acta 318, 415–427.
- Shorttle, O., Maclennan, J., 2011. Compositional trends of Icelandic basalts: implications for short–length scale lithological heterogeneity in mantle plumes. Geochem. Geophys. Geosyst. 12 (11).
- Shorttle, O., Maclennan, J., Lambart, S., 2014. Quantifying lithological variability in the mantle. Earth Planet. Sci. Lett. 395, 24–40.
- Sobolev, A.V., Hofmann, A.W., Sobolev, S.V., Nikogosian, I.K., 2005. An olivine-free mantle source of Hawaiian shield basalts. Nature 434 (7033), 590–597.
- Sobolev, A.V., Hofmann, A.W., Kuzmin, D.V., Yaxley, G.M., Arndt, N.T., Chung, S.-L., Danyushevsky, L.V., Elliott, T., Frey, F.A., Garcia, M.O., et al., 2007. The amount of recycled crust in sources of mantle-derived melts. Science 316 (5823), 412–417.
- Soderman, C.R., Matthews, S., Shorttle, O., Jackson, M.G., Ruttor, S., Nebel, O., Turner, S., Beier, C., Millet, M.-A., Widom, E., et al., 2021. Heavy δ^{57} Fe in ocean island basalts: a non-unique signature of processes and source lithologies in the mantle. Geochim. Cosmochim. Acta 292, 309–332.
- Soderman, C.R., Shorttle, O., Matthews, S., Williams, H.M., 2022. Global trends in novel stable isotopes in basalts: theory and observations. Geochim. Cosmochim. Acta 318, 388–414.
- Soderman, C.R., Shorttle, O., Gazel, E., Geist, D.J., Matthews, S., Williams, H.M., 2023. The evolution of the Galápagos mantle plume. Sci. Adv. 9 (10), eadd5030.
- Sossi, P.A., Nebel, O., Foden, J., 2016. Iron isotope systematics in planetary reservoirs. Earth Planet. Sci. Lett. 452, 295–308.
- Stracke, A., 2012. Earth's heterogeneous mantle: a product of convection-driven interaction between crust and mantle. Chem. Geol. 330, 274–299.
- Stracke, A., Hofmann, A.W., Hart, S.R., 2005. FOZO HIMU, and the rest of the mantle zoo. Geochem. Geophys. Geosyst. 6 (5).
- Stracke, A., Tipper, E.T., Klemme, S., Bizimis, M., 2018. Mg isotope systematics during magmatic processes: inter-mineral fractionation in mafic to ultramafic Hawaiian xenoliths. Geochim. Cosmochim. Acta 226, 192–205.
- Su, B.-X., Hu, Y., Teng, F.-Z., Xiao, Y., Zhang, H.-F., Sun, Y., Bai, Y., Zhu, B., Zhou, X.-H., Ying, J.-F., 2019. Light Mg isotopes in mantle-derived lavas caused by chromite crystallization, instead of carbonatite metasomatism. Earth Planet. Sci. Lett. 522, 79–86.

- Sun, P., Niu, Y., Guo, P., Duan, M., Chen, S., Gong, H., Wang, X., Xiao, Y., 2020. Large iron isotope variation in the eastern Pacific mantle as a consequence of ancient low-degree melt metasomatism. Geochim. Cosmochim. Acta 286, 269–288.
- Teng, F.-Z., Wadhwa, M., Helz, R.T., 2007. Investigation of magnesium isotope fractionation during basalt differentiation: implications for a chondritic composition of the terrestrial mantle. Earth Planet. Sci. Lett. 261 (1–2), 84–92.
- Teng, F.-Z., Dauphas, N., Helz, R.T., 2008. Iron isotope fractionation during magmatic differentiation in Kilauea Iki Lava Lake. Science (ISSN 0036-8075) 320 (5883), 1620–1622. 1095–9203.
- Teng, F.-Z., Li, W.-Y., Ke, S., Marty, B., Dauphas, N., Huang, S., Wu, F.-Y., Pourmand, A., 2010. Magnesium isotopic composition of the Earth and chondrites. Geochim. Cosmochim. Acta 74 (14), 4150–4166.
- Teng, F.-Z., Dauphas, N., Huang, S., Marty, B., 2013. Iron isotopic systematics of oceanic basalts. Geochim. Cosmochim. Acta 107, 12–26.
- Turner, D.L., Jarrard, R.D., 1982. K-Ar dating of the Cook-Austral island chain: a test of the hot-spot hypothesis. J. Volcanol. Geotherm. Res. 12 (3–4), 187–220.
- Wang, W., Wu, Z., Huang, S., Huang, F., 2023. First-principles investigation of equilibrium magnesium isotope fractionation among mantle minerals: review and new data. Earth-Sci. Rev., 104315.
- Wang, X.-J., Chen, L.-H., Hofmann, A.W., Hanyu, T., Kawabata, H., Zhong, Y., Xie, L.-W., Shi, J.-H., Miyazaki, T., Hirahara, Y., et al., 2018. Recycled ancient ghost carbonate in the Pitcairn mantle plume. Proc. Natl. Acad. Sci. 115 (35), 8682–8687.
- Wang, X.-J., Chen, L.-H., Hanyu, T., Shi, J.-H., Zhong, Y., Kawabata, H., Miyazaki, T., Hirahara, Y., Takahashi, T., Senda, R., et al., 2021a. Linking chemical heterogeneity to lithological heterogeneity of the Samoan Mantle Plume with Fe-Sr-Nd-Pb isotopes. J. Geophys. Res., Solid Earth 126 (12), e2021JB022887.
- Weyer, S., Ionov, D.A., 2007. Partial melting and melt percolation in the mantle: the message from Fe isotopes. Earth Planet. Sci. Lett. 259 (1–2), 119–133.
- White, W.M., Duncan, R.A., 1996. Geochemistry and geochronology of the Society Islands: new evidence for deep mantle recycling. Geophys. Monogr.-Amer. Geophys. Un. 95, 183–206.

- White, W.M., Hofmann, A.W., 1982. Sr and Nd isotope geochemistry of oceanic basalts and mantle evolution. Nature 296 (5860), 821–825.
- Willbold, M., Stracke, A., 2006. Trace element composition of mantle end-members: implications for recycling of oceanic and upper and lower continental crust. Geochem. Geophys. Geosyst. 7 (4).
- Williams, H., Prytulak, J., Woodhead, J.D., Kelley, K.A., Brounce, M., Plank, T., 2018. Interplay of crystal fractionation, sulfide saturation and oxygen fugacity on the iron isotope composition of arc lavas: an example from the Marianas. Geochim. Cosmochim. Acta 226, 224–243.
- Williams, H.M., Bizimis, M., 2014. Iron isotope tracing of mantle heterogeneity within the source regions of oceanic basalts. Earth Planet. Sci. Lett. 404, 396–407.
- Woodhead, J.D., Devey, C.W., 1993. Geochemistry of the Pitcairn seamounts, I: source character and temporal trends. Earth Planet. Sci. Lett. 116 (1–4), 81–99.
- Workman, R.K., Hart, S.R., Jackson, M., Regelous, M., Farley, K., Blusztajn, J., Kurz, M., Staudigel, H., 2004. Recycled metasomatized lithosphere as the origin of the Enriched Mantle II (EM2) end-member: evidence from the Samoan Volcanic Chain. Geochem. Geophys. Geosyst. 5 (4).
- Zhao, X., Cao, H.H., Mi, X., Evans, N.J., Qi, Y.H., Huang, F., Zhang, H.F., 2017. Combined iron and magnesium isotope geochemistry of pyroxenite xenoliths from Hannuoba, North China Craton: implications for mantle metasomatism. Contrib. Mineral. Petrol. 172 (6), 40.
- Zhong, Y., Chen, L.-H., Wang, X.-J., Zhang, G.-L., Xie, L.-W., Zeng, G., 2017. Magnesium isotopic variation of oceanic island basalts generated by partial melting and crustal recycling. Earth Planet. Sci. Lett. 463, 127–135.
- Zindler, A., Hart, S., 1986. Chemical geodynamics. Annu. Rev. Earth Planet. Sci. 14 (1), 493–571.